03,08,11

Dependence of AC electrical resistivity on the thickness of the DLC layer in In/DLC//Si/In nanostructure

© I.A. Zur[1], V.Yu. Leonenko[1], A.K. Fedotov[1], E.E. Shmanay[1], A.A. Kharchanka[1], N.I. Gorbachuk[2], E.A. Ermakova[2], S.S. Titova[3], O.A. Chuvenkova[3], S.Yu. Turishchev[3], Yu.A. Fedotova[1], S.A. Movchan[4]

[1] Institute for Nuclear Problems, Belarusian State University, Minsk, Belarus
[2]Department of Physics, Belarusian State University, Minsk, Belarus
[3] Voronezh State University, Voronezh, Russia
[4] Joint Institute for Nuclear Research, Dubna, Russia

E-mail: zur.ilya01@gmail.com

Received November 29, 2024
Revised January 4, 2025
Accepted January 14, 2025

As the thickness of the DLC layer increased from 22 to 46 nm, a corresponding rise in number of carbon atoms with the sp^2 hybridization of electron orbitals from 9% to 21% was observed, by analyzing the X-ray photoelectron spectroscopy (XPS) measurements. Moreover, negligible nitriding and oxidation of the DLC surface was confirmed via X-ray photoelectron spectroscopy. An equivalent electrical circuit is proposed to describe the impedance frequency dependences of the DLC coating as well as the potential barrier at the DLC//Si interface. In the quasistatic limit, the resistivity of the DLC layer decreases from 1000 to 1 $\Omega \cdot$ m as the thickness increases from 22 to 71 nm. It has been demonstrated that the impedance of the In/DLC//Si/In structure can change by a factor of 20 when the bias voltage varies between $-4 - +4$ V relative to the Si substrate.

Keywords: DLC coatings, X-ray photoelectron spectroscopy, impedance spectroscopy, equivalent circuit, zone diagram, electrical resistance.

DOI: 10.61011/PSS.2025.02.60672.324

1. Introduction

DLC (Diamond-like carbon) is a metastable carbon form, whose thermophysical [1], optical [2] and electrophysical [3,4] properties are determined by the ratio of the numbers of atoms with sp^2- and sp^3-hybridization of electron orbitals. DLC coatings are widely used in various industrial applications: wear-resistant coatings [5], antireflection optics [6] and biocompatible coatings [7,8]. Their potential scope of application have been expanded recently — the study of DLC coating application as resistive layers on gas-discharge detector electrodes is currently underway at CERN (European Organization for Nuclear Research) and JINR (Joint Institute for Nuclear Research) [9]. This study covers the investigation of radiation resistance [10] and erosion stability [11] of DLC coatings. In [3], it is shown that DC resistivity of a DLC coating correlates with the alteration of structure as the thickness increases.

Resistive coating of a detector's collecting electrode serves as a distributed thin-film resistor that limits spark discharge current. It is expected that efficiency of such coating will be mainly defined by physical properties such as DC and AC conductivity and permittivity [12].

Therefore, establishment of a correlation between thickness, structure and DC/AC electrical properties of DLC coatings is of absolute importance. Solution of this problem is in combining the methods for investigation of structure and electrical properties of coatings. However, difficulty of this approach is in separating the obtained information about the properties of a substrate and coating itself. For example, DLC coating deposition onto polymer or glass-fabric dielectric substrates precludes the use of Raman scattering spectroscopy (RSS) and infrared spectroscopy for structure investigation. Utilization of a silicon substrate can solve this problem, however, this causes substrate-shunting of the studied DLC coating that has a much higher specific and absolute electrical resistance. In this case, it is correct to measure electrical resistance in a transverse, rather than longitudinal, configuration, which in turn requires consideration of barrier effects at the DLC//Si interface that are caused by energy-band bending.

This study investigates the impedance properties of a In/DLC//Si/In structure and directly of DLC layers. The objective of this study is to establish a correlation between the structure and DC/AC resistivity of DLC coatings.

2. Experimental techniques and equipment

DLC layer samples were deposited onto KDB-8 Si substrates using a technique described in detail in [3]. DLC

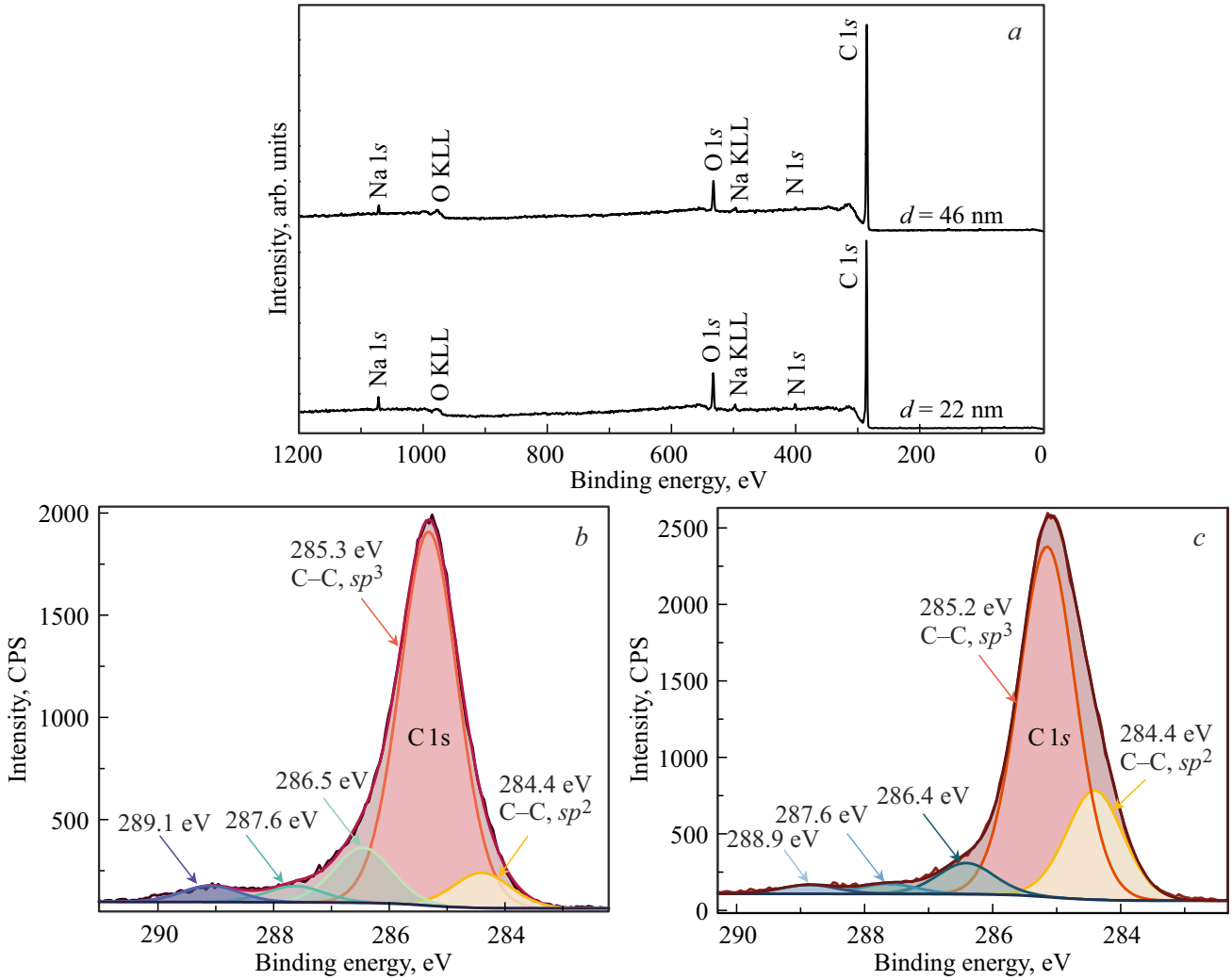

Figure 1. Panoramic XPS spectra of 22 nm and 46 nm DLC coatings (a) and C1s high-resolution XPS spectra of 22 nm (b) and 46 nm (c) DLC coatings. Bond energies of spectrum components are shown in the figure and Table 1.

layer thickness was evaluated by means of contrast analysis of scanning electron microscopy images made using the HITACHI S-4800 microscope.

Physical and chemical state of the sample surface was examined by non-destructive X-ray photoelectron spectroscopy (XPS) using the SPECS Phoibos 150 electron energy analyzer of the ESCA module at the NANOFES ultrahigh-vacuum experimental station of Kurchatov synchrotron, National Research Center „Kurchatov Institute“ (Moscow, Russia) [13]. Monochromatized AlK_α X-ray tube radiation (1486.61 eV) was used. Information-bearing layer depth was from 2 to 3 nm [14] with a resolution of at least 0.1 eV. A standard approach based on independent recording of a signal from pure gold foil (Au4f) was used for spectral normalization and calibration. Spectral lines were identified using the known databases, from which currently existing and most accurate spectra were chosen [14–16].

Impedance-frequency dependences $Z(\nu)$ of the In/DLC//Si/In structure of the DLC coating samples with various thicknesses were measured using the LCR Agilent E4980A system in a probing voltage frequency range from 20 Hz to 2 MHz with the probing sine voltage amplitude not higher than 40 mV. Transverse bias voltage was varied in the range from -4 V to $+4$ V and applied between the indium contacts on the DLC coating and silicon substrate, respectively. All measurements were performed in air at room temperature. Analysis of $Z(\nu)$ was conducted using AfterMath Pine Reseash Instrumentation.

3. Results and discussion

3.1. X-ray photoelectron spectroscopy of DLC coatings

Figure 1, a shows panoramic XPS spectra of 22 nm and 46 nm DLC coatings in the bond energy range from 0 eV to 1200 eV. As the intensity decreases, spectral lines of carbon C1s ($\sim$ 285 eV), oxygen O1s ($\sim$ 531 eV),

Table 1. Results of spectral line decomposition considering sp^2- and sp^3-hybridizations of the electron orbitals of carbon atoms

Thickness, nm	27	46	Literature data
Energy of C1*s* component,eV	C−C sp^2 284.4	C−C sp^2 284.4	284.4 ± 0.1 [16−18]
	C−C sp^3 285.3	C−C sp^3 285.2	285.2 ± 0.1 [16−18]
	286.5	286.4	286.3(sp^2 C−N) [13] 286.4 ± 0.3 (C−O) [17,18] 285.6−286.9 (C−OH) [16]
	287.7	287.6	287.5 (sp^3 C−N) [13] 286.5−287.9 (C=O) [16]
	289.1	288.9	288.4−289.8 (C−OOH) [16] 288.6−289.0 (O−C=O) [19]

sodium Na1*s* ($\sim$ 1072 eV) and nitrogen N1*s* ($\sim$ 398 eV) and Auger lines of KLL Na ($\sim$ 508 eV), KLL O ($\sim$ 984 eV) are observed.

Spectral lines of Na and N feature much lower intensity than that of C and O lines. Na line is probably caused by residual impurities. Minor oxidation and nitriding of the DLC coating surface layer may be treated as a cause of the presence of oxygen and nitrogen lines in the spectrum.

C1*s* spectral lines for 22 nm and 46 nm DLC coatings recorded at high resolution are described in the best way by a set of components shown in Figure 1, *b*, and 1, *c*, that include a signal from carbon atoms with sp^2- and sp^3-hybridization of electron orbitals. Possible states of carbon atoms for the obtained bond energies of the decomposition components are listed in Table 1. Note that the recorded view of C1*s* spectral lines is typical of the samples with both thicknesses.

Potential electron bond energies (see Table 1) correspond to C−O, C=O and C−N and support the previous assumption concerning the DLC surface reconstruction. The obtained electron bond energies $\approx$ 284.4 eV and $\approx$ 285.3 eV for sp^2- and sp^3-hybridizations of the electron orbitals of carbon atoms, respectively, and energy spacing between them demonstrate high degree of agreement with the literature data listed in Table 1.

Figure 2 shows the content of carbon atoms with sp^2-hybridization of electron orbitals $n(\mathrm{C\_}sp^2)$ evaluated by the ratio of C1*s* line decomposition component areas (see Figure 1). Note that the dependence of $n(\mathrm{C\_}sp^2)$ on the DLC coating thickness d (see Figure 2) correlates with the same dependence that was obtained previously for a set of samples in [3] via the Raman scattering spectra analysis. The following possible explanation may be proposed for the increasing trend of the number of carbon atoms with sp^2-hybridization as the DLC coating thickness grows.

Results of simulation of the DLC coating growth on the steel and diamond substrate by the molecular dynamics method are discussed in [20,21]. Results obtained in both

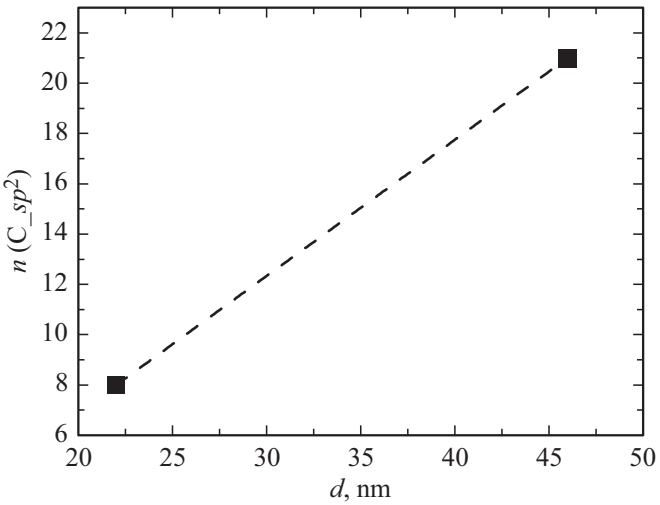

Figure 2. Dependence $n(\mathrm{C\_}sp^2)$ on the DLC coating thickness d.

studies indicate that a $\approx 1.5-2.0$ nm layer consisting of a mixture of substrate and deposited carbon atoms (buffer layer) is formed. Thus, a pure DLC layer is formed on a buffer layer, rather than on the initial substrate. As a consequence, internal stress distribution over the coating thickness is nonuniform. The buffer layer primarily contains atoms with sp^3-hybridization with prevailing compression stresses that reach -10 GPa. With distance from the buffer layer, the fraction of carbon atoms with sp^2-hybridization increases, mechanical stresses change sign and reach 9 GPa.

Thus, as the DLC coating grows, contribution of the potential profile of the Si substrate and SiC buffer layer directly to the DLC layer formation decreases, which increases the probability of C localization in the configuration corresponding to a less strained structure. Such minimization of internal stresses in the system might be attained through the increase in the number of carbon atoms with sp^2-hybridization of electron orbitals.

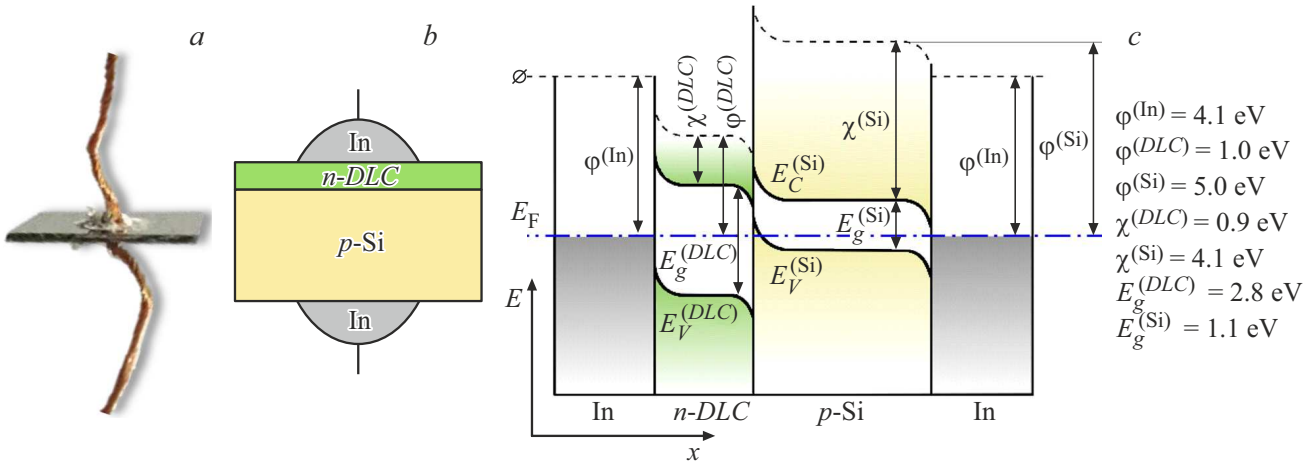

Figure 3. Photo (a), schematic diagram (b) and band diagram (c) of the In/DLC//Si/In structure.

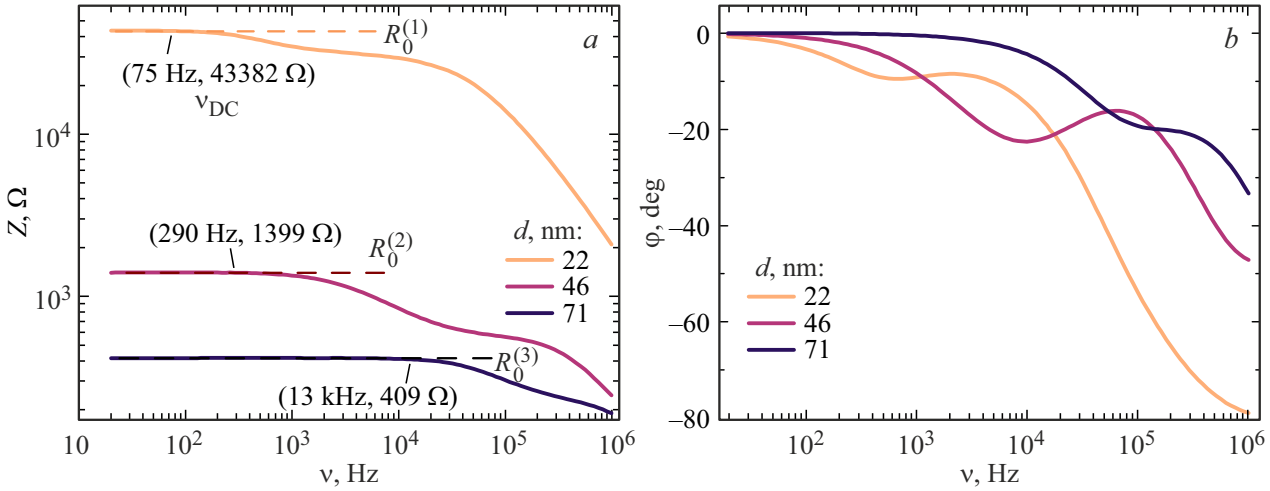

Figure 4. Frequency dependences of the impedance $Z(\nu)$ (a) and phase angle $\varphi(\nu)$ (b) of the In/DLC//Si/In structure on the basis of 22 nm, 46 nm and 71 nm DLC layers obtained at $T = 293$ K.

3.2. Impedance spectroscopy of the In/DLC//Si/In structure

Photo and schematic diagram of the studied In/DLC//Si/In structure are shown in Figures 3, a and 3, b, respectively. The first layer of the structure is a DLC coating with the electron type of conductivity [3,4], the second layer consists of a Si substrate with p-type conduction [22]. Band gap E_g of DLC coatings varies from 2 eV to 3 eV [18,23], for p-Si, E_g is equal to 1.1 eV [24]. Taking into account the difference in the type and concentration of charge carriers, and vacuum work functions (φ_{DLC} and φ_{Si}) in DLC and Si, occurrence of an energy barrier may be suggested at the DLC//Si interface due to the alignment of the Fermi level E_F in the system in the equilibrium state (without external electric field). Schematic energy band diagram in the structure equilibrium state indicating the system-specific E_F, φ_{DLC} and φ_{Si} for DLC and Si is shown in Figure 3, c.

The full impedance $Z(\nu)$ of the structure is defined by the sum of impedances of the structural components (impedance $Z_{DLC}(\nu)$ of the DLC layer, impedance $Z_{Barrier}(\nu)$ of the DLC//Si barrier and impedance $Z_{Si+cont}(\nu)$ of the substrate with electrical contacts):

$$Z(\nu) = Z' + iZ'' = Z_{Si+cont}(\nu) + Z_{DLC}(\nu) + Z_{Barrier}(\nu), \quad (1)$$

where Z' and Z'' are real and imaginary components of the impedance Z, respectively.

Figure 4, a and 4, b shows the frequency dependences of the impedance $Z(\nu)$ and phase angle $\varphi(\nu)$ of the In/DLC//Si/In structure consisting of 22 nm, 46 nm and 71 nm DLC layers. It can be seen that in the low frequency limit ($\nu \to 0$), the scalar impedance tends to a constant value of R_0 and is defined by a sum of active components $Z_{DLC}(\nu)$ and $Z_{Barrier}(\nu)$

$$Z(\nu \to 0) = R_0 = \mathrm{Re}(Z_{Si+cont}) + \mathrm{Re}(Z_{DLC}) + \mathrm{Re}(Z_{Barrier}). \quad (2)$$

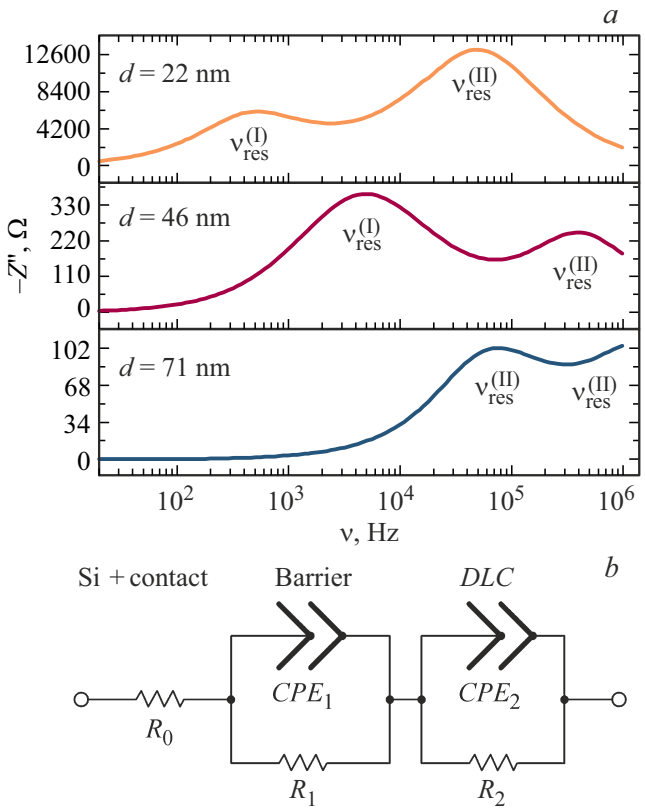

Figure 5. Frequency dependence of the imaginary component of impedance $-Z''$ (a) and equivalent scheme (b) of the In/DLC//Si/In structure.

At the same time, $\varphi(\nu \to 0)$ takes on values next to zero, which in total indicates that there is no contribution of the capacitive component to the full impedance of the structure.

As the DLC coating thickness increases, frequency ν_{DC}, at which the system response to the probing voltage is similar to the response to DC, shifts to the high frequency region. As shown in Figure 4, a, deviation of Z from R_0 is observed at 75 Hz for a sample with 22 nm DLC coating and at $\nu_{DC} = 13$ kHz for a sample with $d = 71$ nm. However, $Z(\nu)$ doesn't provide any information concerning the electrical properties of the DLC layer itself.

It follows from Figure 5, a that two resonances (maxima) are distinguished on $-Z''(\nu)$: low-frequency ($\nu_{res}^{(I)}$ from 0.5 kHz to 68 kHz) and high-frequency ($\nu_{res}^{(II)}$ from 80 kHz to 480 kHz), that correspond to the barrier and DLC layer terms in relation (1). The more the DLC layer thickness the higher values are taken by ν_{DC}, $\nu_{res}^{(I)}$ and $\nu_{res}^{(II)}$.

According to the energy band diagram (see Figure 3, c) and $-Z''(\nu)$ of the In/DLC//Si/In structure, it is expected that there are two series-connected R/CPE-loops in the equivalent circuit (EC) (see Figure 5, b). These loops describe Z' and Z'' components of the energy barrier impedance at the DLC//Si interface and DLC coating itself. Resistance of the contacts and Si substrate is defined by the resistance element R_0. By determining the ES parameters (see Figure 5, b), dependence of Z_{DLC} and its resistivity ρ on thickness d may be obtained.

Constant phase element CPE in the equivalent scheme makes it possible to account for the effect of DLC//Si interface morphology on the geometrical capacity [25]. The goodness-of-fit χ^2 for approximation of $Z(\nu)$ by the equivalent cirquit with CPE element is equal to approx 0.003, compared with $\chi^2 \approx 0.683$ for the scheme with capacitor

$$Z(CPE) = \frac{1}{\omega^{\alpha} C}, \tag{3}$$

where $\alpha = 1$ describes a frequency dependence of the capacitor C, $\alpha \in 0.8-1.0$ corresponds to a so-called „fractal capacitor" [25].

Figure 6, a–c shows frequency dependences of full impedance $Z_{full}(\nu)$ of the In/DLC//Si/In structure, barrier subloop impedance $Z_{Barrier}(\nu)$ and DLC layer subloop $Z_{DLC}(\nu)$. At the probing voltage frequencies $\nu < \nu_{DC}$ for the 22 nm and 46 nm DLC coating samples, Z_{DLC} is much higher than $Z_{Barrier}$ and only for the sample with $d = 71$ nm $Z_{DLC} < Z_{Barrier}$.

The inset in Figure 6, a shows the impedance hodographs $-Z''$ vs Z' of the In/DLC//Si/In structure, that represent a pair of overlapping semicircles, which indicates that the charge relaxation times of DLC and DLC//Si barrier are close to each other. The centers of semicircles are in the low and high frequency region, which, on curve $Z(\nu)$ (see Figure 5, a), corresponds to the first $\nu_{res}^{(I)}$ and second $\nu_{res}^{(II)}$ resonances of R/CPE-loops describing the barrier and DLC coating.

As shown in Figure 6, d, both the DLC coating impedance and barrier impedance decrease with the growth of d. $Z_{Barrier}(\nu)$ tends to a constant value. Frequency dependences of Z''_{DLC} and Z'_{DLC} are provided in the appendix.

Table 2 shows the values of the equivalent cirquit component parameters for the In/DLC//Si/In structure obtained according to the hodographs.

The In/DLC//Si/In structure is asymmetric in type and concentration of charge carriers. This expectedly suggests

Table 2. Equivalent scheme parameters of the In/DLC//Si/In structure

Parameter	Thickness		
	22 nm	46 nm	71 nm
CPE_1, nF	41.2	1.2	6.7
α_1	0.94	0.97	0.83
CPE_2, nF	0.4	124.0	16.1
α_2	0.89	0.88	1
R_0, Ω	9.93	78.23	0.1
R_1, Ω	12 190	472.5	249.8
R_2, Ω	31 750	860.3	166.6

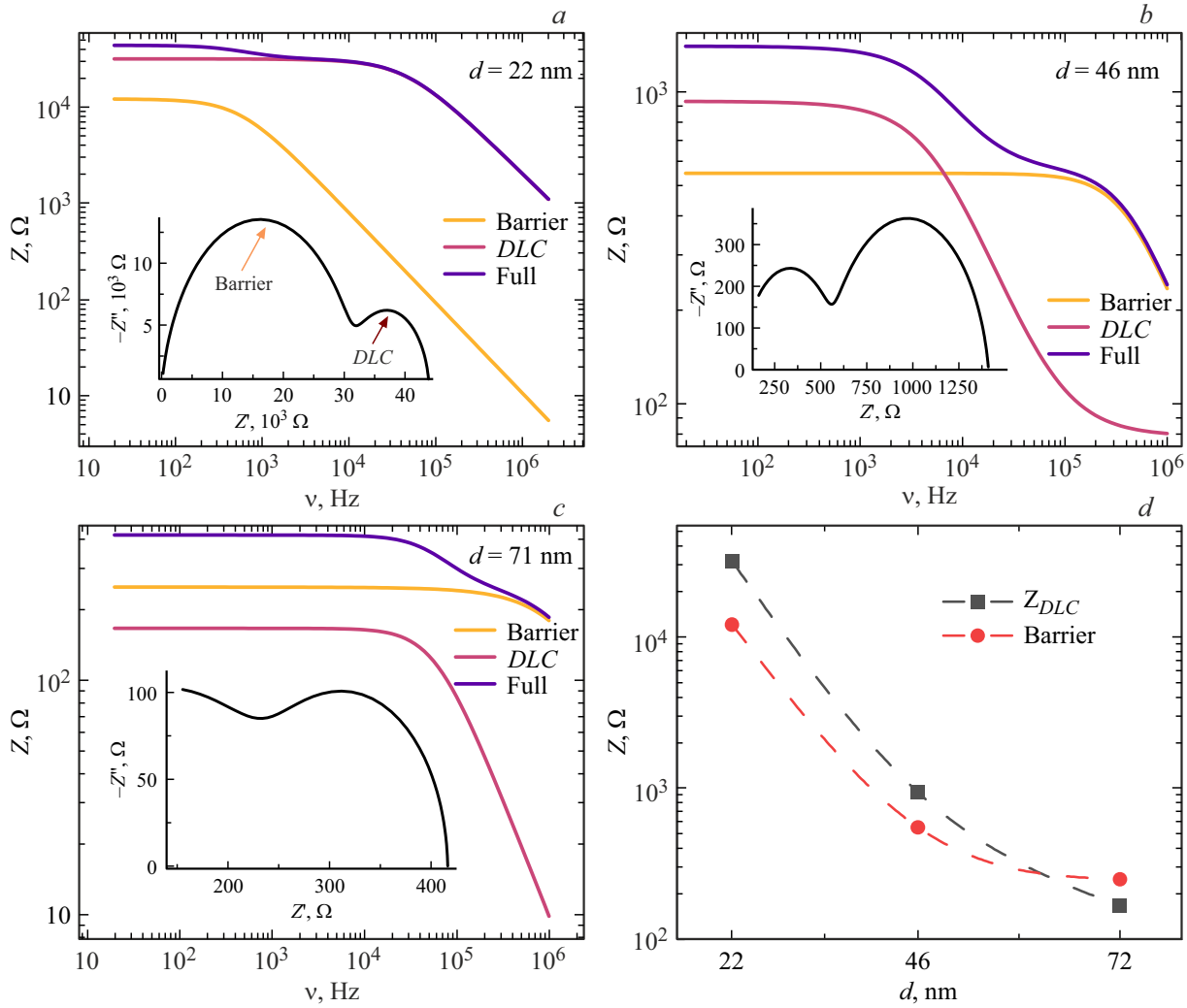

Figure 6. (a–c) — Frequency dependences of the full impedance of the In/DLC//Si/In structure $Z_{full}(\nu)$, and of contributions to the subloop impedances $Z_{Barrier}(\nu)$ and Z_{DLC} for 22 nm (a), 46 nm (b) and 71 nm (c) DLC layers; d — dependences of $Z_{Barrier}$ and Z_{DLC} on d at $\nu = 20$ Hz.

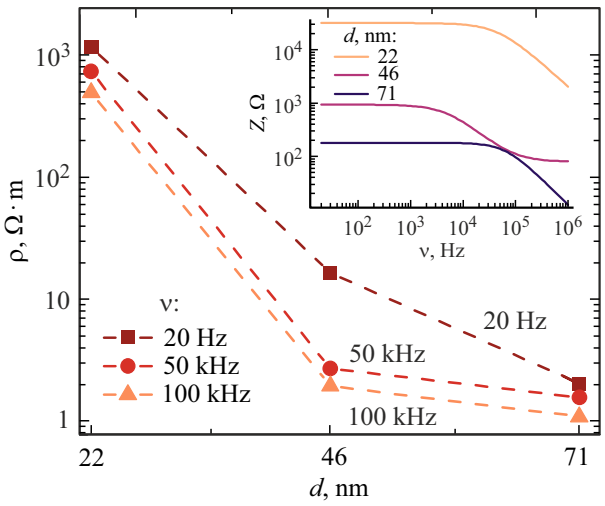

Figure 7. Dependence of the DLC layer resistivity on d. The inset shows the frequency dependences of the full impedance of 22 nm, 46 nm and 71 nm DLC coating.

that its impedance (Z_{full}) depends on the polarity and amplitude of the transverse bias voltage U_{bias}. Let's assume the structure to be forward-biased, if $U_{bias} > 0$ V is applied to the Si substrate (and $U_{bias} < 0$ V applied to the DLC layer, respectively) and to be reverse-biased, when $U_{bias} < 0$ V is applied to the Si substrate.

3.3. Dependence of the In/DLC//Si/In parameters on the bias voltage

Figure 8, a–c shows that the increase in U_{bias} in the reverse-biased scheme is followed by the growth of Z_{full} with $\nu < \nu_{DC}$. One resonance gradually disappears on curves $Z(\nu)$, and only one semicircle is distinguished on the impedance hodographs (see Figure 8, d–f). It is suggested that $Z_{Barrier}$ increases and the contribution of Z_{DLC} becomes insignificant. Increase in U_{bias} in the forward direction, on the contrary, leads to barrier suppression and, consequently, to the decrease in Z_{full}.

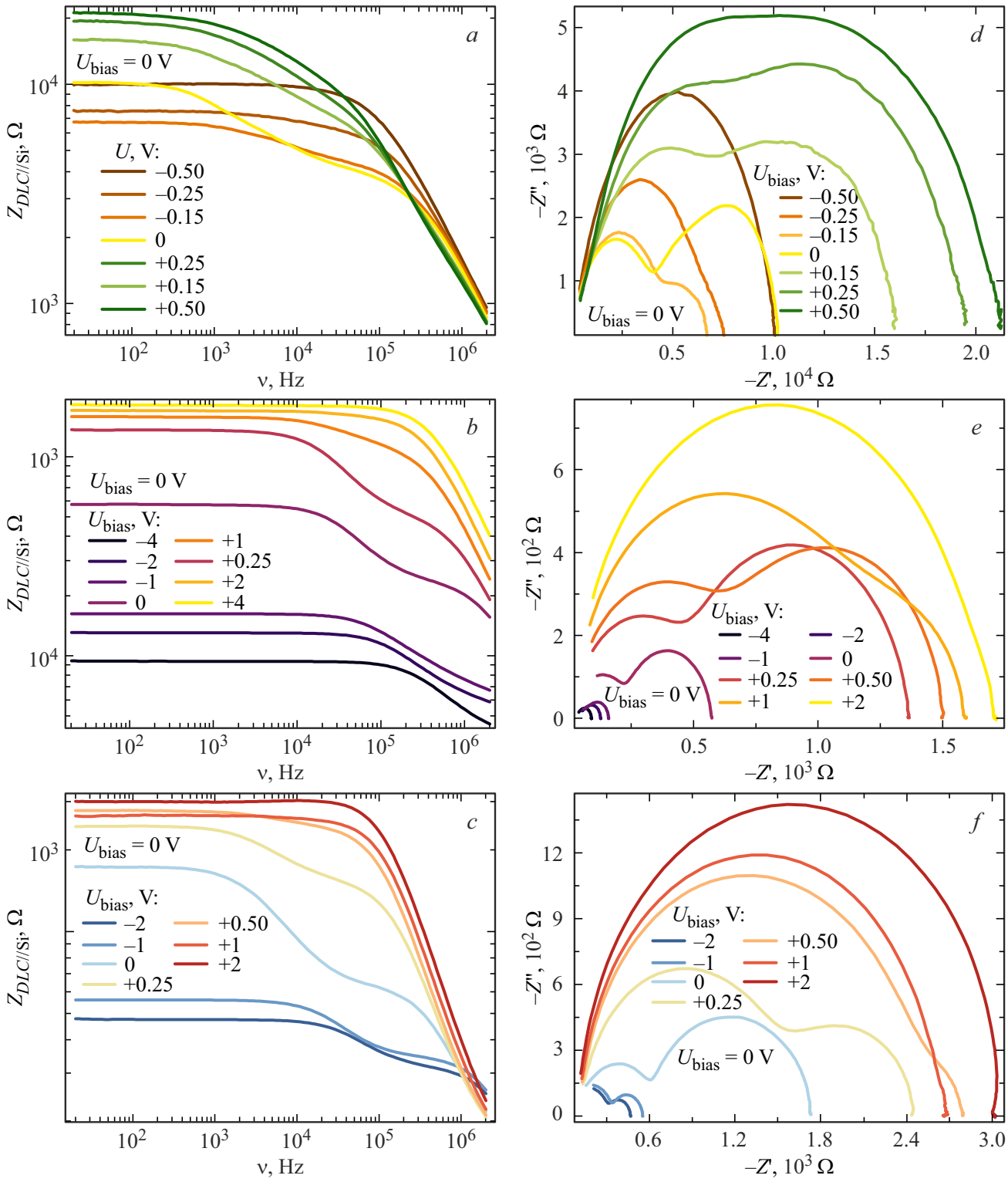

Figure 8. Frequency dependence Z_{full} $(a–c)$ and impedance hodographs $(d–f)$ of the In/DLC//Si/In structure consisting of 22 nm, 46 nm and 71 nm DLC layers, respectively.

Table 3. Parameters of approximation by function (4) of curves $Z(U_{bias})$ for 22 nm, 46 nm and 71 nm DLC layer samples

d, nm	22	46	71
Z_{min}, Ω ($U_{bias} = -4$ V)	9811	94 ± 11	410 ± 6
Z_{max}, Ω ($U_{bias} = +4$ V)	14787	1816 ± 22	2914 ± 12
U_1, V	–	0.075 ± 0.005	-0.005 ± 0.004
U_2, V	–	0.83 ± 0.16	0.49 ± 0.04
k_1, V	–	-0.07 ± 0.01	-0.10 ± 0.005
k_2, V	–	-0.93 ± 0.09	-0.82 ± 0.03
p	–	0.67 ± 0.02	0.59 ± 0.01

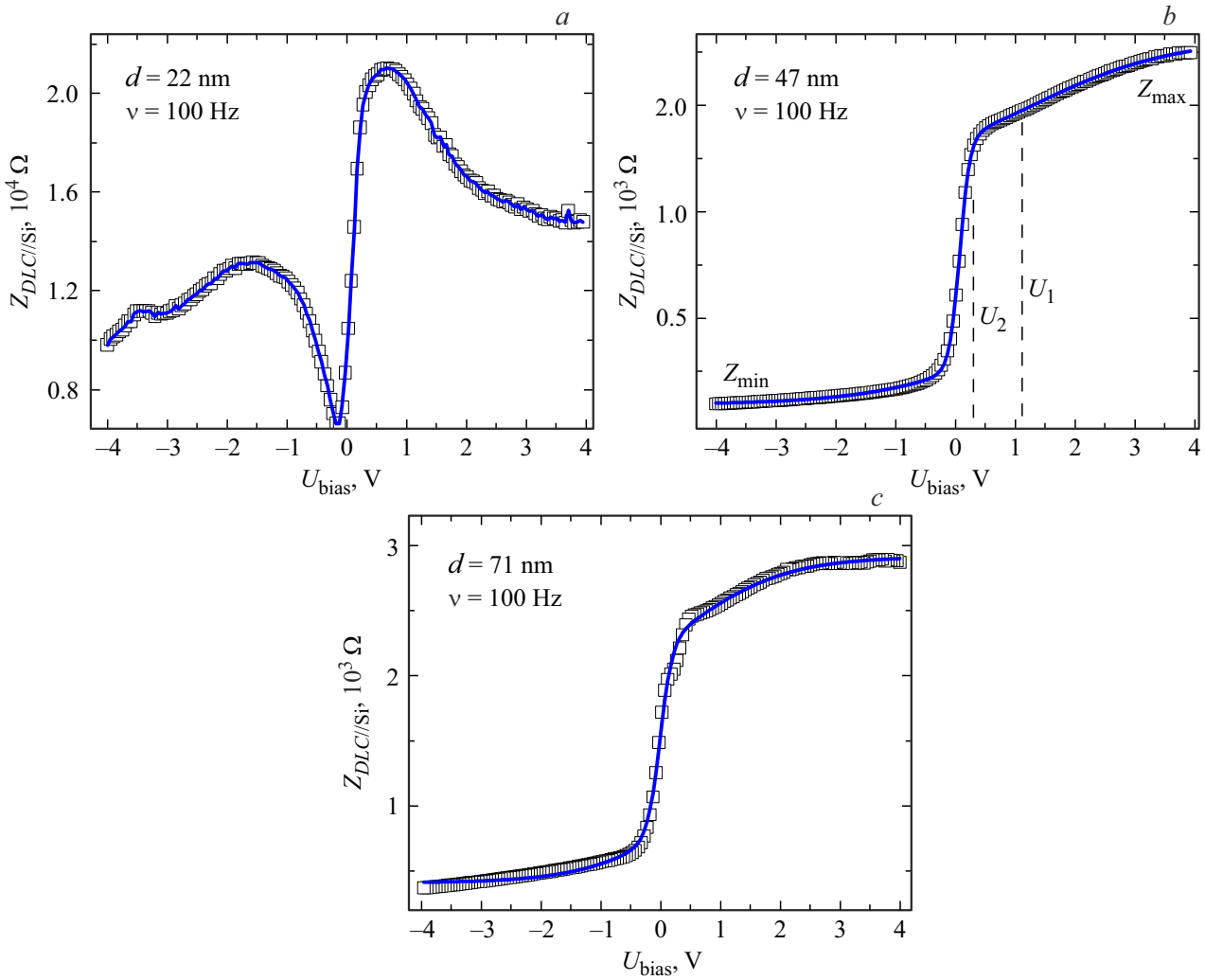

Figure 9. Dependence of Z_{full} of the structure on U_{bias} with the probing voltage frequency of 100 Hz for structures with 22 nm (a), 46 nm (b) and 71 nm (c) DLC layers.

Figure 9 shows the dependence of Z_{full} on the amplitude of U_{bias} applied to the structure at the probing voltage frequency $\nu = 100\,\text{Hz}$. Depending on the polarity U_{bias}, Z_{full} is characterized by two limits: $Z_{\min}$ for forward bias and $Z_{\max}$ for reverse bias, which is generally similar to the behavior of $p-n$-transition on the open and closed state.

For the 46 nm and 71 nm DLC samples, curves $Z(U_{\text{bias}})$ for the In/DLC//Si/In structure at $\nu = 100\,\text{Hz}$ may be approximated by function (4), the approximation parameters are listed in Table 3.

$$Z(U_{\text{bias}}) = Z_{\min} + A\left[\frac{p}{1 + e^{(U_{\text{bias}}-U_1)/k_1}} + \frac{1-p}{1 + e^{(U_{\text{bias}}-U_2)/k_2}}\right], \tag{4}$$

where $Z_{\min}$ is the impedance limit for the structure in the „open“ state $A = Z_{\max} - Z_{\min}$ is the difference between the impedance limits of the structure in the „forward-biased“ and „reverse-biased“ states, p is the contribution of the first and second subsystems to the full impedance, U_1 and U_2 are the bias voltages, at which $0.5A$ is reached for the first and second subsystems, respectively, k_1 and k_2 are the parameters defining the slope of curve.

For the 22 nm DLC structure, starting from $|U_{\text{bias}}| > 1.5\,\text{V}$, Z_{full} has a decreasing tendency regardless of the bias voltage polarity. Such behavior that differs from the 46 nm and 71 nm samples may be interpreted as a consequence of electron injection from the indium electrodes or Si substrate.

Dependence of the DLC coating resistivity ρ on d (contribution of Z_{Barrier} is removed) at the probing voltage frequencies from 20 Hz to 100 kHz (Figure 7) correlates with that in [3].

As the bias voltage increases in the positive direction ($U_{\text{bias}} > 0\,\text{B}$ is applied to Si), the spatial charge region gets larger near the DLC//Si interface and, consequently, the Z_{Barrier} component in (1) makes the main contribution to the full impedance of the structure. Accordingly, one R/CPE-loop describing the DLC coating impedance can be excluded from the substitution cirquit because $Z_{\text{Barrier}} \gg Z_{\text{DLC}}$.

When a negative voltage ($U_{\text{bias}} < 0\,\text{V}$) is applied to DLC, full impedance of the structure decreases, on the contrary, with respect to Z ($U_{\text{bias}} = 0\,\text{V}$), which is explained by the barrier suppression and injection of non-equilibrium charge carriers from the indium electrode or Si substrate into the DLC layer [3]. With such scheme, ES remains unchanged.

4. Conclusion

Analysis of the X-ray photoelectron spectroscopy (XPS) data of nanoscale DLC coatings confirms the increase in the number of carbon atoms with sp^2-hybridization of electron orbitals from 8% to 21 % as the thickness increases from 22 nm to 46 nm. It was found that DLC surface layer atoms form chemical bonds C−O, C=O and C−N, which indicates minor oxidation and nitriding of DLC during reconstruction after opening the vacuum chamber.

Study of the full impedance, imaginary and real parts in the In/DLC//Si/In structure in the frequency range from 20 Hz to 2 MHz made it possible to form an electrical equivalent cirquit. The proposed ES consists of two series-connected R/CPE-loops and a series resistance, and makes it possible to factor the contributions to the full impedance of the DLC//Si potential barrier and DLC layer. ES takes a form of hodographs consisting of two unresolved semicircles, whose parameters depend on the DLC layer thickness and bias voltage. Analysis of the equivalent scheme component parameters that an increase in the DLC layer thickness from 22 nm to 71 nm leads to a decrease in resistivity from 1000 to $1\,\Omega \cdot \text{m}$ in the quasi static limit.

Response of the In/DLC//Si/In impedance to the bias voltage is similar to the behavior of $p-n$-transition in the forward-biased and reverse-biased states. This is explained by the formation of a potential barrier at the DLC//Si interface due to the difference in the type and concentration of charge carriers in the DLC layer and Si substrate. As a consequence, the In/DLC//Si/In impedance may vary by a factor of 20 depending on the polarity and amplitude of bias voltage that controls the spatial charge parameters at the DLC//Si interface.

The obtained results suggest that the DLC layer resistivity in a wide range of electrical field frequencies is unambiguously defined by the concentration of carbon atoms with sp^2-hybridization of the electron orbitals. By manipulating the polarity and amplitude of external bias voltage, the In/DLC//Si/In structure parameters may be controlled. The results may be useful for creating GEM detectors with resistive coating of the collecting electrode.

Acknowledgments

The study was partially funded within the national research program „Photonics and Electronics for Innovations“, 2021−2025, „Microelectronics and nanoelectronics“) Reg. No. 20212560. X-ray photoelectron spectroscopy examination was supported by the Ministry of Science and Higher Education of Russia under Agreement No. 075-15-2021-1351. The authors are grateful to A.V. Larkin, senior lecturer of the Department of Physics of Solid Body and Nanotechnology, for discussion of the findings.

Funding

The work was supported by the Belarusian Republican Foundation for Fundamental Research (agreement F23M-099.

Conflict of interest

The authors declare that they have no conflict of interest.

Appendix

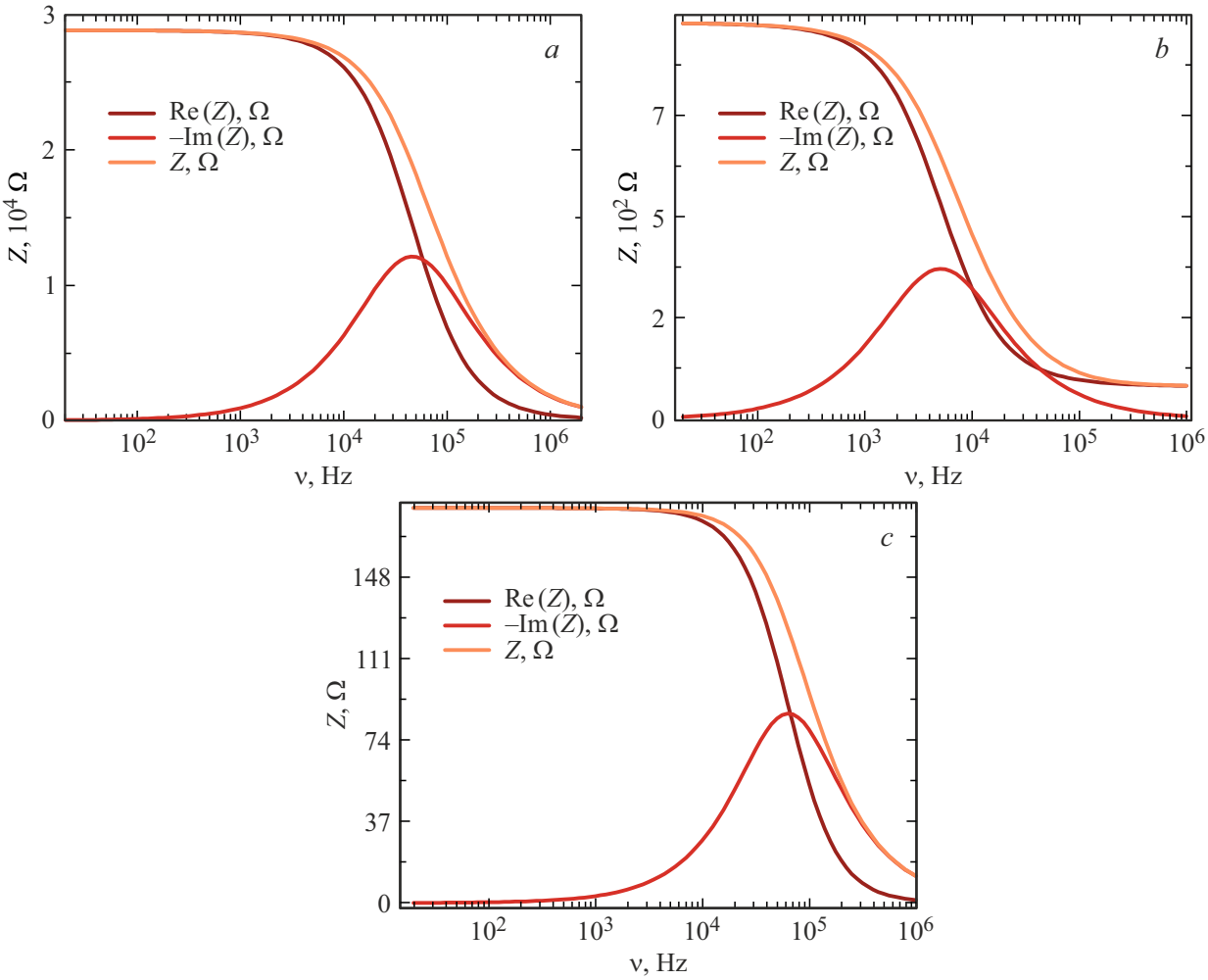

Figure A1. Frequency dependence of impedance $Z_{DLC}(\nu)$, imaginary Z'' and real Z' impedance components for the 22 nm (a), 46 nm (b) and 71 nm (c) DLC layers.

References

[1] M. Shamsa, W. Liu, A. Balandin, C. Casiraghi, W. Milne, A. Ferrari. Appl. Phys. Lett. **89**, 161921 (2006).

[2] F. Stock, F. Antoni, F. Le Normand, D. Muller, M. Abdesselam, N. Boubiche, I. Komissarov. Appl. Phys. A **123**, 590 (2017).

[3] I.A. Zur, E.E. Shmanai, Yu.A. Fedotova, A.A. Kharchenko, S.A. Movchan. FTT **65**, 49 (2023). (in Russian).

[4] A. Grill, V. Patel, S. Cohen. Diam. Relat. Mater. **3**, 281 (1994).

[5] http://www.dlc.ru/oblasti-primeneniya/detali-i-mehanizmy/.

[6] C.R. Lin, D.H. Wei, C.K. Chang, W.H. Liao. Phys. Procedia **18**, 46 (2011).

[7] P.A.Avgustovsky. Innovatsionnye tekhnologii i obrazovanie — 2022 — S. 288–291. (in Russian).

[8] Y. Deng. https://proleantech.com/ru/dlc-coating-comprehensive-guide/.

[9] J. Metcalfe, I. Mejia, J. Murphy, M. Quevedo, L. Smith, J. Alvarado, B. Gnade, H. Takai. arXiv:1411.1794 [Hep-Ex, Physics:Physics] (2014).

[10] A.A. Kharchenko, I.A. Zur, Yu.A. Fedotova, Khimiya vysokikh energiy **56**, 378 (2022). (in Russian).

[11] I. Zur, Y. Shmanay, J. Fedotova, G. Remnev, S. Movchan, V. Uglov, Diam. Relat. Mater. **142**, 110802 (2024).

[12] I.A. Zur, A.S. Fedotov, A.A. Kharchanka, Y.E. Shmanay, J.A. Fedotova, S.A. Movchan. Nonlinear Phenomena in complex systems **26**, *4*, 393–400 (2023).

[13] Y.S. Zou, Q.M. Wang, H. Du, G.H. Song, J.Q. Xiao, J. Gong, C. Sun, L.S. Wen. Appl. Surf. Sci. **241**, 295 (2005).

[14] C.K. Park, S.M. Chang, H.S. Uhm, S.H. Seo, J.S. Park. Thin Solid Films **420–421**, 235 (2002).

[15] N. Dwivedi, S. Kumar, H.K. Malik, Govind, C.M.S. Rauthan, O.S. Panwar, Applied Surface Science **257**, 6804 (2011).

[16] B. Lesiak, N. Rangam, P. Jiricek, I. Gordeev, J. Tóth, L. Kövér, M. Mohai, P. Borowicz, Front. Chem. **7** (2019).

[17] P. Mérel, M. Tabbal, M. Chaker, S. Moisa, J. Margot. Appl. Surf. Sci. **136**, 105 (1998).

[18] H. Sheng, W. Xiong, S. Zheng, C. Chen, S. He, Q. Cheng. Carbon Lett. **31**, 929 (2021).

[19] F. Xiao, W. Li, L. Fang, D. Wang. J. Hazard. Mater., **308**, 11 (2016).

[20] W. Xiaoqiang, Z. Xu, H. Xiangyi, T. Yingjian, W. Haojie, F. Haoran, L. Huimin. Sci. Rep. **14** (2024).
[21] N. Kametani, M. Nakamura, K. Yashiro, T. Takaki. Comput. Mater. Sci. **209**, 111420 (2022).
[22] https://russkijmetall.ru/redkozemelnyy-metall-i-dr/kremniy-metallicheskiy/kremniy-kristallicheskiy/kremniy-monokristallicheskiy/plastiny-kremniya-monokristallicheskogo-kef/.
[23] A. Evtukh, V.G. Litovchenko, M. Strikha, A. Kurchak, O. Yilmazoglu, H. Hartnagel. Ukr. J. Phys. **62**, 526 (2017).
[24] L. Hao, Y. Liu, W. Gao, Z. Han, Q. Xue, H. Zeng, Z. Wu, J. Zhu, W. Zhang. J. Appl. Phys. **117**, 114502 (2015).
[25] Yu.V. Emelyanova, M.V. Morozova, Z.A. Mikhailovskaya, E.S. Buyanova. Impedansnaya spektroskopiya: teoriya i primenenie (Izdatelstvo Uralskogo universiteta, Yekaterinburg, 2017). (in Russian).

Translated by E.Ilinskaya